Postharvest Biology and Technology 52 (2009) 189–195

Contents lists available at ScienceDirect

Postharvest Biology and Technology

journal homepage: www.elsevier.com/locate/postharvbio

Assessment of tomato pericarp mechanical damage using multivariate analysis of magnetic resonance images

Rebecca R. Milczarek[a], Mikal E. Saltveit[b], T. Casey Garvey[c], Michael J. McCarthy[a,*]

[a] Department of Biological & Agricultural Engineering, University of California, Davis, One Shields Avenue, Davis, CA 95616, USA
[b] Department of Plant Sciences, University of California, Davis, One Shields Avenue, Davis, CA 95616, USA
[c] ConAgra Foods Research and Development, Davis, CA 95616, USA

ARTICLE INFO

Article history:
Received 1 May 2008
Accepted 1 January 2009

Keywords:
Tomato
Mechanical damage
Multivariate image analysis
Magnetic resonance imaging (MRI)
Sorting

ABSTRACT

During steam peeling, severely bruised tomatoes will disintegrate, leading to loss of product. The overall purpose of this study was to develop an in-line method to detect damaged pericarp tissue in processing tomatoes. Magnetic resonance (MR) imaging methods characterize the environment of water protons in plant tissue, resulting in contrast between image pixels corresponding to bruised and sound tissue. Many types of MR imaging protocols are available; in this study, the multivariate image analysis (MIA) method of partial least squares (PLS) was used to determine the optimal MR pulse sequences for tomato pericarp damage assessment. A set of 13 congruent MR images of each of 112 processing tomatoes was used for prediction. The images were created by varying key parameters in 4 different MR pulse sequences. These multivariate images were used to predict the pixel intensities in regions of interest (ROIs) corresponding to the pericarp of the tomato. The pixels in the ROIs for each tomato sample were assigned a value between 0 (no damage) and 1 (extensive damage), corresponding to the conductivity score for that sample, measured after imaging. PLS models of 1–13 latent variables were generated, and cross validation was performed. The root mean square error of cross validation (RMSECV) of the PLS models leveled off after 8 latent variables, so this model was used for conductivity score prediction. The 8 latent variable model captured 97% of the variance in the independent variable (the MR images) and 54% of the variance in the dependent variable (the conductivity scores). The Variable Importance in Projection scores for the 13 MR image sequence types in the chosen model indicated that the Fast Spin Echo sequence with receiver gain of 10 and Turbo Fast Low-Angle Shot sequences with inversion times of 400 ms, 800 ms, 1000 ms, and 1200 ms had the strongest influence on the model. The root mean square error of calibration (RMSEC) and RMSECV of a final model including only these five sequences were low: 0.16 and 0.17, respectively. Thus, MIA of MR images of tomato proved to be effective for predicting the conductivity score of pericarp tissue in tomatoes.

Published by Elsevier B.V.

1. Introduction

1.1. Mechanical damage in tomatoes

The commercial process for canning whole-peeled tomatoes involves several steps that can cause mechanical damage to the fruit. Gondolas of mechanically harvested fruit are water-dumped into flumes, which gives the fruit an initial washing and serves as a transport medium. After multiple drops and rounding several corners in the flumes, the fruit are fed to a steam peeler via a vertical conveyor. By the time fruit have reached the peeler, they are likely to have sustained many impacts resulting in varying degrees of bruising. During the harsh steam peeling process, severely bruised fruit will disintegrate, leading to loss of product. Removing damaged fruit from the feed stream before peeling will reduce this loss and divert fruit to other more appropriate products, such as sauce or paste. An added advantage of such a diversion is that the sauce or paste made from unpeeled fruit will have higher viscosity (and, as a result, higher value) than that made from peeled fruit.

Some damaged fruit, such as those with large cracks in the skin, are obvious upon visual inspection and could be sorted by hand. However, the worldwide impact of viscosity loss and labor associated with hand sorting is estimated to be $100 million USD per year (T. Casey Garvey, personal communication). In addition, some fruit appearing to be sound are heavily damaged. It would be difficult to sort these fruit by color or visual appearance because bruising does not cause sufficiently detectable changes in these attributes. The purpose of this study was to develop a method to detect damaged tissue, specifically pericarp tissue, in intact tomatoes.

* Corresponding author. Tel.: +1 530 752 8921; fax: +1 530 752 4759.
E-mail addresses: rmilczar@ucdavis.edu (R.R. Milczarek), mjmccarthy@ucdavis.edu (M.J. McCarthy).

0925-5214/$ – see front matter. Published by Elsevier B.V.
doi:10.1016/j.postharvbio.2009.01.002

1.2. Magnetic resonance imaging

Magnetic resonance (MR) methods can detect and characterize the environment of water protons in plant tissue. Hills and Remigereau (1997) demonstrated that water in three compartments of a plant cell (vacuole, cytoplasm, and cell wall) could be differentiated based on MR transverse relaxation time, T_2. Several studies have shown that internal browning and core breakdown (disorders associated with breakdown of cell membranes) can be detected in apples (Clark and Burmeister, 1999; Gonzalez et al., 2001) and pears (Lammertyn et al., 2003; Hernández-Sánchez et al., 2007) using MR images. In mango fruit, spin-echo MR imaging can identify mesocarp tissue damaged by disinfestation heat treatment (Joyce et al., 1993). Bruising in whole apples, peaches, pears, and onion was seen in images obtained from a 2 T superconducting magnet system (Chen et al., 1989). Thus, we expected that MR images would provide sufficient contrast to identify different levels of damage in tomato tissue.

However, natural biological variation makes image-based quantification of damaged tissue a difficult task. MR imaging is a promising technology for this task, but a single MR image type may not be sufficient to characterize the entire spectrum of damage levels possible in tomato pericarp. Combining information from two or more differently weighted MR images introduces a multivariate advantage and makes classification more efficient. In this study, multivariate image analysis (MIA) was the method used to determine which MR images to use and in what manner to use them.

1.3. Multivariate image analysis

MIA is an extension of standard multivariate statistical techniques to image-based data sets. A multivariate image is a set of multiple congruent images of the same object. Each individual image may be obtained in any number of ways; in this case, images were obtained using different MR pulse sequences. By "unwrapping" multivariate images row-by-row or column-by-column, these images can be analyzed in the same ways as regular multivariate data sets. Multivariate statistical techniques such as principal components analysis, partial least squares (PLS), and cluster analysis are applied to the unwrapped data set, and the results are rewrapped to create new images that are then interpreted statistically.

MIA has already been applied to multi- and hyper-spectral image data sets of agricultural commodities (e.g. El Masry et al., 2007). Geladi and Grahn (1996) suggested that MIA could be used for MR image data sets, but at present there are no published applications of MIA for MR imaging in postharvest handling.

In the present study, PLS was the specific MIA technique used to interpret the data. PLS is an iterative technique that seeks to maximize the explanation of variance in both the X-block (the data that is used for prediction) and the Y-block (the figure of merit that is being predicted). The result of PLS is a model for creation of a prediction image. The prediction image is a linear combination of k images, where k is the number of individual images making up the multivariate image.

1.4. Conductivity test

The overall strategy of this study was to create a PLS model that, when applied to a multivariate MR image of tomato pericarp, would generate a score on a continuum of 0 (no damage) to 1 (extensive damage). A localized, quantitative, continuous measurement of pericarp damage was required in order to implement this strategy. Sensory evaluation, i.e. squeezing the fruit, would be rapid and as quantitative as a well-designed scale would allow, but it would not be sufficiently localized. A compression test, such as that used by Tu et al. (2007) for tomato firmness measurement, would give information on the fruit as a whole, but again would not be localized. A nondestructive firmness tester based on a pneumatically operated impact head equipped with a piezoelectric sensor was used by Valero et al. (2007) to assess the firmness of various stone fruits; such a sensor would likely provide localized firmness measurement of tomatoes as well. However, the use of any of these techniques presumes that firmness (as measured through the fruit epidermis) is correlated with mechanical damage. While this is a sound assumption, a technique that more directly measures the extent of cell damage was desired. The conductivity test was the technique used for this purpose.

The conductivity test assesses membrane permeability via the measurement of ion leakage from the plant tissue into a surrounding solution (Saltveit, 2000). Ion leakage measurements have previously been used in a number of applications, including quantifying chilling injury in cucumbers (Kuo and Parkin, 1989) and tomatoes (Saltveit, 2002) and mechanical damage to popcorn kernels (Goneli et al., 2007). Commonly, a disk of plant tissue is excised from a sample and immersed in an isotonic solution of a sugar such as mannitol or sucrose. Due to concentration gradients between the tissue and surrounding solution, ions flow out from the plant cells and into the solution. The resulting change in electrolytic conductance of the solution is monitored with a conductivity meter. The SI units of this measurement are siemens per meter (S/m). Distilled water has a conductivity in the range of 0.1–1 mS/m, while conductivities of solutions in equilibrium with plant tissues are 1–2 orders of magnitude larger.

It was expected that the leakiness of tomato pericarp samples, as measured by an ion leakage score, would result in distinctive contrast patterns in MR images. Thus, the objective of this study was to predict conductivity scores of tomato pericarp samples by MIA applied to a series of MR images.

2. Materials and methods

2.1. Sample collection and MR imaging

Samples of California processing tomatoes were obtained during 7 weeks of the 2007 harvest season. For each of 7 batches, 8 heavily bruised (skin intact) and 8 non-bruised (firm) fruit were manually selected from tomatoes on a conveyor in the ConAgra tomato processing plant in Oakdale, CA. (The purpose of this sampling procedure was to ensure that the samples spanned the entire damage spectrum.) Tomatoes on the conveyor had been washed and color sorted, but had not been sorted for other characteristics. In general, the samples were imaged the day after they were obtained from the processing plant, and the conductivity measurements made the day after imaging. In some cases, the samples were imaged on the same day they were obtained from the plant.

Each individually numbered tomato was inserted into the bore of a 1 T industrial-grade MR imaging system (Aspect AI; Netanya, Israel), with the stem/calyx axis along the (horizontal) bore. Each fruit was manually centered in the 70 mm bore using a plastic half-tube sample holder. The image slice was the center X–Y slice, which had a thickness of 17 mm (Fig. 1). The field of view for all the images was 68 mm × 68 mm.

Thirteen MR images were obtained for each sample. The MR pulse sequences employed to produce these images, chosen for their speed and contrast features, are summarized in Table 1. The Fast Spin Echo (FSE) image had an effective echo time of 281 ms and produces T_2-weighted contrast in the images. The Gradient Recalled Echo (GRE) sequence, with its short echo time and repetition time yields proton density weighting. The Turbo FLASH sequence, a Fast Low-Angle Shot sequence with an inversion pulse at the beginning, yields weighting based on longitudinal relaxation time (T_1). The GRE sequence was actually a 64-slice 3D sequence; the central 16

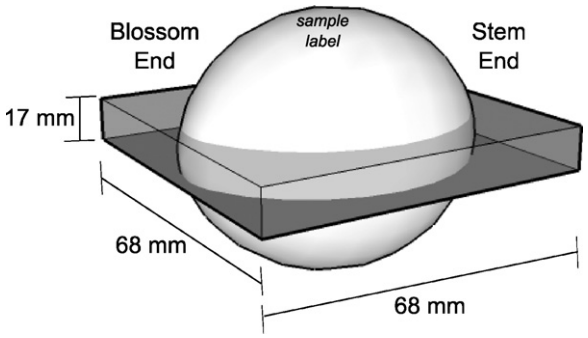

Fig. 1. Perspective diagram of tomato and image area orientation—not to scale. The dark gray slab represents the magnetic resonance (MR) image area for each tomato sample.

slices of this set were combined in post-processing to create a single image that was congruent to the other 12.

It would not be feasible to adjust the receiver gain for each fruit in an in-line regime. Thus, the receiver gain on the FSE sequence was varied to determine if this parameter significantly affected the contrast between damaged and sound tissue. At gain levels of 16 and 18, images of some samples were showing signs of saturation, so 18 is near the upper limit on receiver gain for FSE images on tomato on this particular MR system. The inversion pulse time (TI) in the Turbo FLASH sequence was varied from 200 ms to 1200 ms in steps of 200 ms; this enabled comparison of the T_1s of damaged and sound tissue within the framework of the MIA. For reference, 4 (out of 13) images of a heavily bruised fruit are shown in Fig. 2.

2.2. Conductivity measurement

After imaging, pericarp samples were analyzed in the conductivity test. An isotonic solution of 0.25 mol/L sucrose was used for the conductivity measurements. The isotonic concentration was determined by an initial gravimetric experiment, as per the procedure of Saltveit (2002).

A metal borer was used to excise 2 cylindrical pericarp tissue samples from each side of the fruit. Each excised sample was trimmed with a razor blade so that the resulting disk was 1 cm in diameter and 0.4 cm in thickness. The sample was first trimmed just below the epidermis and then trimmed a second time to achieve the desired disk thickness. Two disks were obtained from the central third of the left side of the fruit and two from the right side, "left" and "right" being relative to the label. Thus, four disks were obtained from each fruit. The two disks from each side were rinsed

Table 1
MR image types.

Pulse sequence name	Receiver gain (arbitrary gain units)	Inversion time (ms)
Turbo FLASH[a]	80	200
FSE[b]	10	
GRE[c]	50	
FLASH	80	
Turbo FLASH	80	400
FSE	12	
Turbo FLASH	80	600
FSE	14	
Turbo FLASH	80	800
FSE	16	
Turbo FLASH	80	1000
FSE	18	
Turbo FLASH	80	1200

[a] Fast Low-Angle Shot.
[b] Fast Spin Echo.
[c] Gradient Recalled Echo.

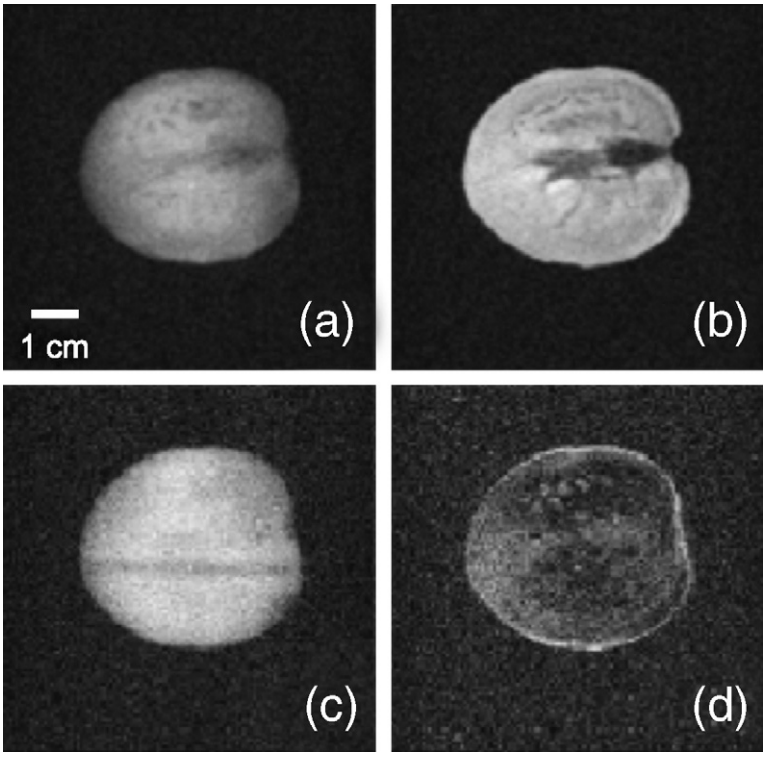

Fig. 2. Example magnetic resonance (MR) images of a damaged sample. All images depict the same plane of the fruit and have the same field of view (68 mm × 68 mm) and resolution (1.1 mm/pixel), but were generated by different MR pulse sequences. The MR pulse sequences represented are Fast Spin Echo with Receiver Gain = 10 (a), central slice of 3D Gradient Recalled Echo (b), Fast Low-Angle Shot (c), and Turbo Fast Low-Angle Shot with inversion time = 800 ms (d). All pericarp in this fruit was damaged.

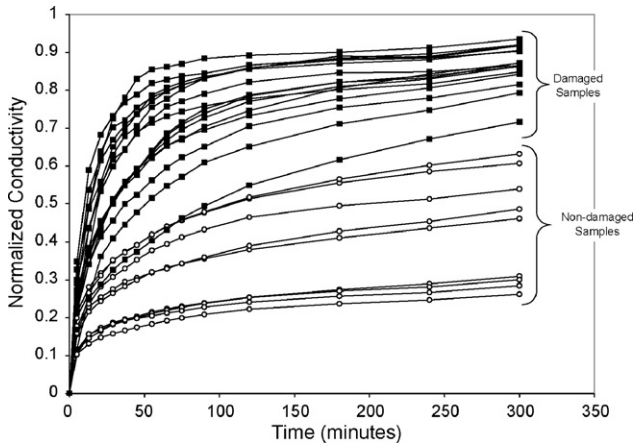

Fig. 3. Conductivity measurements for bruised and sound pericarp samples.

with the 0.25 mol/L sucrose solution, drained, patted dry with a paper towel, and placed in a labeled Petri dish for ease of identification and handling. When all 64 disks (16 fruit × 2 sides per fruit × 2 disks per side) were prepared, 32 × 50 mL culture tubes were each filled with 20 mL of 0.25 mol/L sucrose solution. The conductivity of these solutions was measured in μS/cm using the probe of a Fisher Scientific conductivity meter (Model 09-326-2). An initial conductivity was recorded, and timing started when the two disks for each sample were dropped into the corresponding culture tube. Conductivity measurements were taken periodically for the next 300 min. The interval between measurements was short (5–8 min) at the beginning of the run and longer (60 min) near the end. The rack of tubes was agitated at 2 s^{-1} on a laboratory shaker platform between measurements. After the final measurement, the culture tubes were capped and placed in a −62 °C freezer overnight. The next day, the frozen samples were removed from the freezer and warmed to ca. 20 °C. After a second overnight freeze/thaw cycle, a conductivity measurement was taken and used as the "total conductivity". The conductivity values over time for each sample were divided by the sample's total conductivity to obtain a unit-less measurement of conductivity that varied from 0 to 1. The unit-less conductivity measurement at 240 min was used as the "conductivity score" because the conductivity measurements appeared to level off at this time point. Fig. 3 depicts the conductivity measurements for one of the batches.

2.3. PLS modeling

An MIA PLS model was devised to predict the conductivity score. A partial-annular region of interest (ROI) was selected for each side of a fruit image. This ROI size and shape was chosen so that only the pericarp tissue that would have been excised to supply the disks for the conductivity measurement was used as the basis for the model. All other parts of the image were ignored. Example ROIs are shown in Fig. 4.

For each of the 13 MR images, the average values of the pixels covered by this ROI were used as the X-block for the PLS model. Again, the conductivity score, the quantity to be predicted the model, was used as the Y-block. The PLS model was determined using Matlab® (r2006b; The Mathworks; Natick, MA) MIA_Toolbox (Eigenvector Research, Inc.; Wenatchee, WA). The data in both the X- and Y-block were pre-processed subtracting the mean and dividing by the standard deviation of each variable, reducing the influence of large magnitude and variance data points on the model.

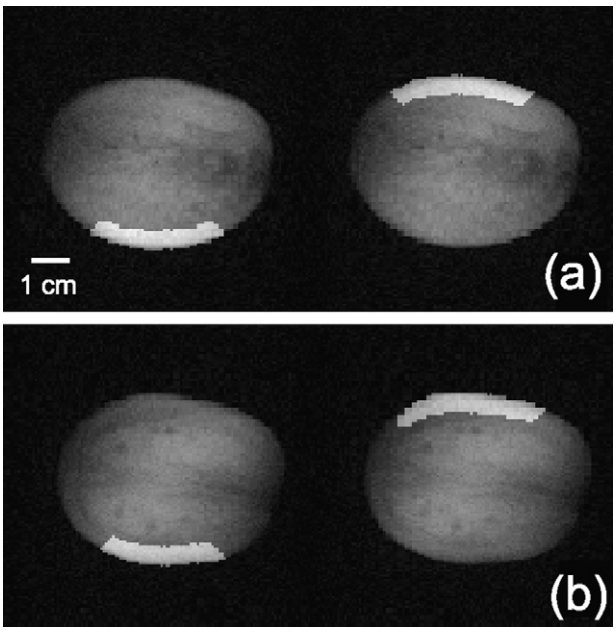

Fig. 4. Example regions of interest (ROIs) selected for two different fruit, overlaid on the Fast Spin Echo image. Left (left) and Right (right) side ROIs for a firm sample (a) and a soft sample (b). Pixels in the ROIs corresponded to tissue excised for the conductivity test and were used for multivariate image analysis. Field of view = 68 mm × 68 mm and resolution = 1.1 mm/pixel.

3. Results and discussion

3.1. PLS model for entire sample set

Leave-one-out cross validation was performed to determine how many latent variables to include in the final PLS model. That is, for each cross validation step, a PLS model was generated using a calibration set of 223 of the 224 samples, and the remaining sample was used as a test set. The root mean square error of cross validation (RMSECV) of the PLS models leveled off at 0.18 after 8 latent variables, so this model was used for conductivity score prediction. The 8 latent variable model captured 97% of the variance in the X-block (the mean pixel values of the ROIs in the MR images) and 54% of the variance in the Y-block (the conductivity scores). Example prediction images for two typical sound and damaged fruit are shown in Fig. 5a. Hyper-intense pericarp pixels represent areas of high conductivity score (i.e. extensive membrane damage), while hypo-intense pericarp pixels correspond to sound tissue. Note that, from this model, no claim is made about the integrity of the cells in other tissues of the fruit, e.g. locular gel and columella.

Fig. 6a is a plot of the predicted versus measured scores for all 224 samples. This depicts the performance of a PLS model constructed from all available samples, as would be the case in an unsupervised sorting situation in a processing plant. However, some X-block and Y-block information used to create this model was probably faulty. As previously mentioned, the FSE images of some fruit showed signs of saturation at receiver gains of 16 and 18, so the FSE images of these fruit at high gains contain contrast patterns that should not be modeled. Also, a software malfunction caused some images in Batch 7 to have vertical stripes, again producing images that should not be used in the X-block. Several fruit in Batches 1, 5, and 6 had measured conductivity scores that were greater than 1 (see Fig. 6a). For Batch 1, this result can be attributed to poor agitation of the samples before the final conductivity reading; unless the sample tubes were shaken vigorously by hand just prior to measurement, a temperature gradient was visible in the liquid. The conductivity meter is temperature-sensitive, so such a

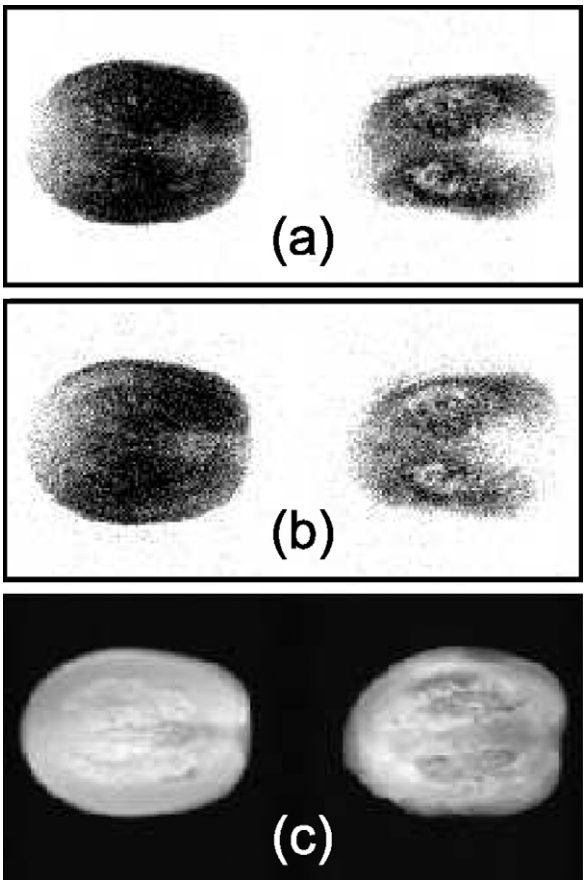

Fig. 5. Prediction images for two example fruit. Prediction images generated from the 8-Latent Variable Partial Least Squares model based on the 224-sample set (a) and the abridged sample set (b). The Gradient Recalled Echo images of the two fruit are included in (c) for reference of the positions of the fruit. For each model, the images are of a firm fruit (left) and a soft fruit (right); note hypo-intense, non-damaged pericarp tissue in the firm fruit and hyper-intense, damaged pericarp tissue in the soft fruit. Field of view = 68 mm × 68 mm and resolution = 1.1 mm/pixel.

gradient would be expected to alter the results of the measurement. The technique was refined to include manual agitation for Batches 2 and later. For Batches 5 and 6, conductivity instrument drift was evident from measurement of a blank solution (sucrose solution with no tomato tissue) before the sample measurements at each time point. Although the raw conductivity measurements were scaled according to the drift evident in the blank solution, this resulted in some conductivity scores being higher than 1. This problem could be reduced by measuring a standard solution at each time point or using a more stable conductivity meter. The latter approach was successfully used in a subsequent study (data not shown) during the 2008 harvest season.

3.2. PLS model for abridged sample set

Therefore, the data from fruit affected by any of the three above-mentioned problems were discarded, and a new PLS model was constructed based on the abridged data set. Example prediction images and the predicted vs. measured plot for this new model are shown in Figs. 5b and 6b, respectively. The model (also with 8 latent variables) captured 98% of the variance in the X-block and 49% of the variance in the Y-block. The root mean squared error of calibration (RMSEC) for the new model was 0.15 (compared to 0.16 for the original model), and the RMSECV was 0.18 (compared to 0.18). Thus, the model constructed using the abridged data set performed similarly well to the original model. This indicates that the MR images and conductivity measurements need not be "perfect" to construct a useful MIA model.

For both the full data set and abridged data set, the model tends to under-predict the conductivity scores of highly damaged samples, as evidenced by the vertical cluster of points in Fig. 6a and b near measured conductivity = 1. This indicates that the MR images used for this analysis may be appropriate for predicting pericarp damage up to a point but that heavy damage results in variation that these MR images do not capture. The solution to this would be to use other MR image types to augment the model. Also, there may be more subtle levels of tissue damage at the high end of the scale that the conductivity test does not indicate. Nevertheless, the low values of RMSEC and RMSECV indicate that the present PLS models are sufficient for predicting conductivity scores from the 13 MR image types used in this study.

In a PLS model, Variable Importance in Projection (VIP) scores quantify which variables (in this case, image sequence types) contribute most strongly to the prediction image. Plots of the VIP scores for the 13 MR image sequence types are shown in Fig. 7. For the original model (all 224 samples included), the MR image sequences that had VIP scores above 1 were the FSE sequence at receiver gain

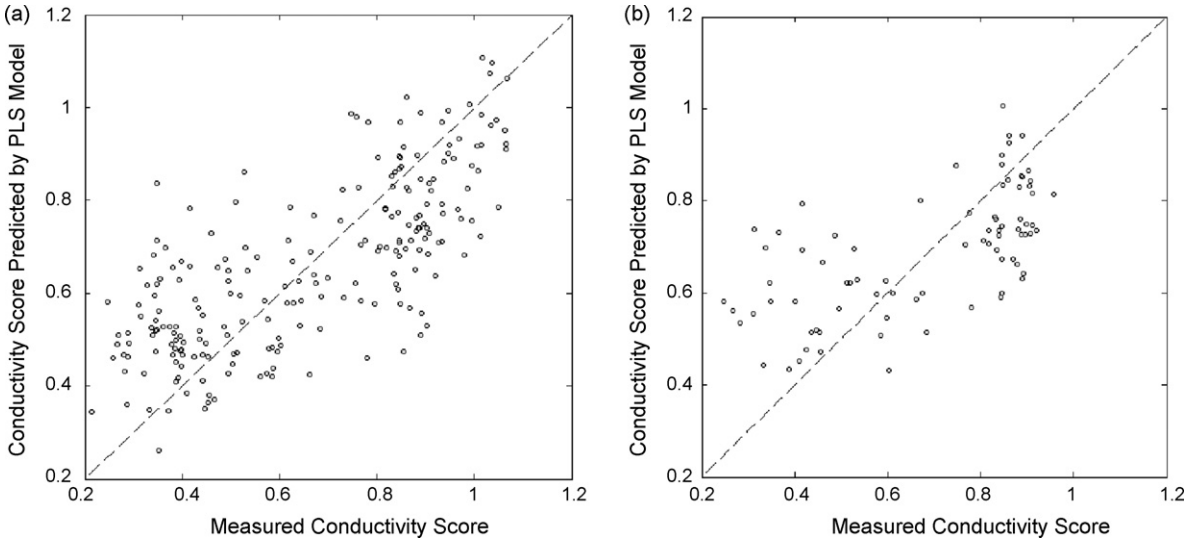

Fig. 6. Predicted conductivity score versus measured conductivity score. The scores are plotted for the two partial least squares models based on the 224-sample set (a) and the abridged sample set (b).

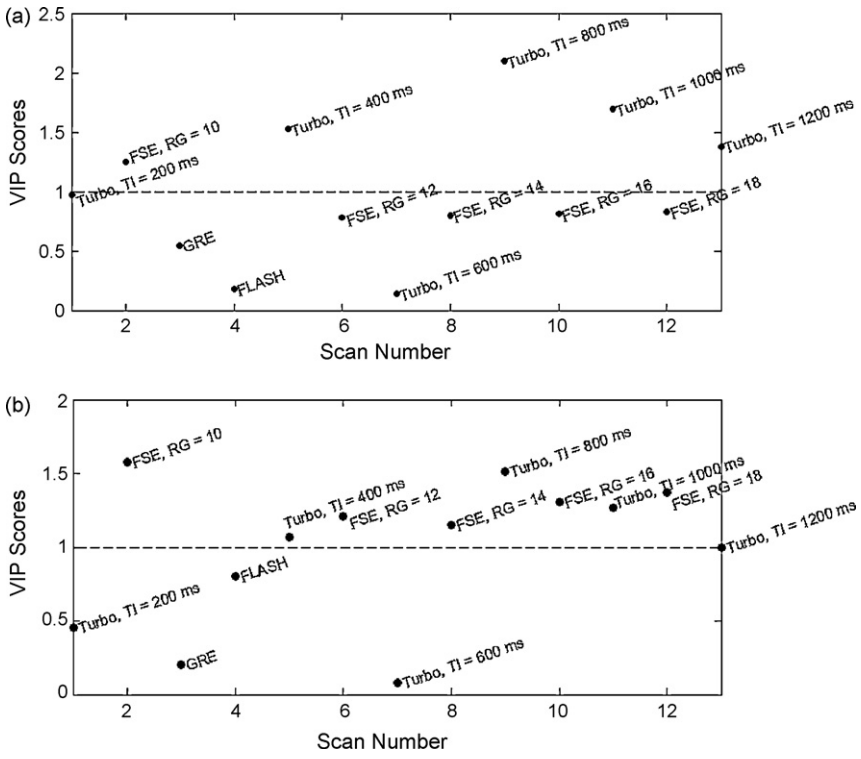

Fig. 7. Variable Importance in Projection (VIP) scores for different pulse sequences. The VIP scores are plotted for the two partial least squares models based on the 224-sample set (a) and the abridged sample set (b).

(RG) = 10 and the Turbo FLASH sequences with TI = 400 ms, 800 ms, 1000 ms, and 1200 ms. The images from these sequences had the greatest influence on the PLS model. This indicates that the other 8 imaging sequences were less important in the model and could be excluded.

The fact that the FSE sequence had a high VIP score at RG = 10 but not at the other RG levels is surprising. All the FSE images for each fruit had similar contrast patterns and thus would be expected to contribute equally to the model. The most likely reason for the high influence of the FSE sequence at RG = 10 is the fact that the ROIs were constructed based on this image. Thus, the pixels from which the X-block data were obtained were most closely matched up with those from the FSE, RG = 10 image. It is possible, due to frequency drift over time, that the 13 images of each fruit were not perfectly congruent. An image with proportionately more pixels included in the ROI would thus have high influence on the model. The frequency drift occurs due to temperature variations in the magnet; permanent magnet-based MRI systems are known to have this problem (Aspect AI, personal communication). Thus, two solutions are suggested: temperature control of the magnet or more frequent checking and resetting of the central frequency (which, in the present experiment, was reset for every sample but not for every image).

With the exception of the FSE, RG = 10 image sequence, FSE sequences for which the receiver gain was varied all had similar, low VIP scores. This indicates that receiver gain does not have a strong influence on the prediction of conductivity score from FSE sequences. It was surprising that the FSE sequence did not have a stronger influence on the model. The T_2 contrast produced by this sequence was expected to be a source of differentiation between damaged and sound tissue.

For the model based on the abridged data set (Fig. 7b), the FSE sequences did have VIP scores greater than 1. Their VIP scores were all about the same, with the exception of the score of the RG = 10 sequence, which may have undue influence on the model for reasons stated earlier. This confirms that receiver gain does not affect the ability of the FSE sequence to predict conductivity scores.

Future method development will focus on the sequences with the highest VIP scores. Since the Turbo FLASH sequence had such a large influence on the model, it is likely that conductivity scores can be predicted by differences in the T_1 relaxation times of sound and damaged tissue. According to the VIP scores from the abridged model, the FSE sequence also contributes to the prediction of conductivity scores. In a practical application, the receiver gain would be set as low as possible to prevent saturation. So, even though the FSE sequence at higher receiver gain settings had high VIP scores with the abridged model, the five sequences that warrant further investigation are FSE at RG = 10 and Turbo FLASH at TI = 400 ms, 800 ms, 1000 ms, and 1200 ms.

4. Conclusions

To verify that a model that includes only the five high-VIP-score sequences would still accurately predict conductivity scores, a third PLS analysis was run on the abridged data set. The resulting model (made using only the "top five" sequences) produced the predicted conductivity scores shown in Fig. 8. The pattern in this plot and the model's RMSEC and RMSECV values (0.16 and 0.17, respectively) indicate that the accuracy of the regression analysis was not adversely affected by excluding the other 8 image types.

If all five sequences with high VIP scores were run for each fruit, the total imaging time would be less than 5 s. This is still an order of magnitude longer than an imaging time appropriate for in-line implementation, but there are some options available for reducing this time. The resolution could be lower than that of the images in this study (approximately 1 pixel/mm) and still retain sufficient spatial information for sorting. One could also include fewer

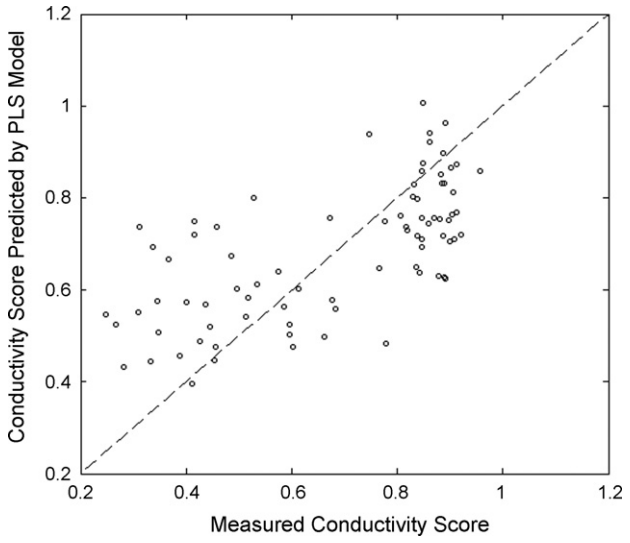

Fig. 8. Predicted conductivity score versus measured conductivity score for five sequence model. The image data set that generated these scores was comprised of the Fast Spin Echo image at receiver gain (RG) = 10 and the Turbo Fast Low-Angle Shot image with inversion time (TI) = 400 ms, 800 ms, 1000 ms, and 1200 ms.

sequences to reduce the imaging time, but this would decrease the accuracy of the model. Therefore, there is a time/accuracy tradeoff that should be considered when implementing this sort of a model in a production environment.

In such an environment, the five MR images of the each fruit would be combined, according to the PLS model, to create a damage prediction image. A pixel histogram analysis of this prediction image would place each fruit in a spectrum of damage levels and direct the fruit on to steam peeling or off the line for other uses. Alternatively, the PLS model could be used to direct the development of a single MR pulse sequence that would have high contrast between sound and damaged tissue. The feasibility of such a sequence remains an open question.

In general, MIA of MR images of tomato proved to be effective for predicting the conductivity score of pericarp tissue in tomatoes. Future development of this technique will relate MRI-measured membrane integrity to other relevant quality indices, such as peel-ability (for processing tomatoes). The present analysis was performed only on tomato pericarp tissue, and it is possible that cell membrane integrity in other tissues would have an effect on peel-ability. For example, the state of the epidermis, especially at its attachment point on the stem scar, may also affect peel-ability. The cross-sectional area of tomato epidermis is very small relative to the length scales that can be achieved with current MR imaging systems. Thus, multivariate MR imaging would not be an appropriate technique for assessing peel-ability if the epidermis were the most important tissue for peel-ability. However, at present, the conductivity score of the pericarp (as predicted by MIA of MR images) promises to be a strong indicator of peel-ability, so MR imaging, in turn, promises to be an effective on-line tool for tomato peel-ability assessment.

Acknowledgements

The authors gratefully acknowledge the financial support of the United States Department of Agriculture Cooperative State Research, Education, and Extension Service, National Research Initiative proposal number 2007-02632. We also thank ConAgra Foods for providing tomato samples and research support staff.

References

Chen, P., McCarthy, M.J., Kauten, R., 1989. NMR for internal quality evaluation of fruits and vegetables. Trans. ASAE 32, 1747–1753.

Clark, C.J., Burmeister, D.M., 1999. Magnetic resonance imaging of browning development in 'Braeburn' apple during controlled-atmosphere storage under high CO_2. Hortscience 34, 915–919.

El Masry, G., Wang, N., El Sayed, A., Ngadi, M., 2007. Hyperspectral imaging for nondestructive determination of some quality attributes of strawberry. J. Food Eng. 81, 98–107.

Geladi, P., Grahn, H., 1996. Multivariate Image Analysis. John Wiley & Sons Ltd., New York.

Goneli, A.L.D., Correa, P.C, Resende, O., Reis Neto, S.A., 2007. Electrical conductivity for quality evaluation of popcorn kernels subjected to mechanical damage. Biosys. Eng. 96, 361–367.

Gonzalez, J.J., Valle, R.C., Bobroff, S., Biazi, W.Z., Mitcham, E.J., McCarthy, M.J., 2001. Detection and monitoring of internal browning development in 'Fuji' apples using MRI. Postharvest Biol. Technol. 22, 179–188.

Hernández-Sánchez, N., Hills, B.P., Barreiro, P., Marigheto, N., 2007. An NMR study on internal browning in pears. Postharvest Biol. Technol. 44, 260–270.

Hills, B.P., Remigereau, B., 1997. NMR studies of changes in subcellular water compartmentation in parenchyma apple tissue during drying and freezing. Int. J. Food Sci. Technol. 32, 51–61.

Joyce, D.C., Hockings, P.D., Mazucco, R.A., Shorter, A.J., Brereton, I.M., 1993. Heat treatment injury of mango fruit revealed by nondestructive magnetic resonance imaging. Postharvest Biol. Technol. 3, 305–311.

Kuo, S., Parkin, K.L., 1989. Chilling injury in cucumbers (*Cucumis sativa* L.) associated with lipid peroxidation as measured by ethane evolution. J. Food Sci. 54, 1488–1491.

Lammertyn, J., Dresselaers, T., Van Hecke, P., Jancsók, P., Wevers, M., Nicolaï, B.M., 2003. Analysis of the time course of core breakdown in 'Conference' pears by means of MRI and X-ray CT. Postharvest Biol. Technol. 29, 19–28.

Saltveit, M.E., 2000. Discovery of chilling injury. In: Kung, S.D., Yang, S.F. (Eds.), Discoveries in Plant Biology, vol. 3. World Scientific Publishing, Singapore, pp. 423–448.

Saltveit, M.E., 2002. The rate of ion leakage from chilling-sensitive tissue does not immediately increase upon exposure to chilling temperatures. Postharvest Biol. Technol. 26, 295–304.

Tu, S.S., Choi, Y.J., McCarthy, M.J., McCarthy, K.L., 2007. Tomato quality evaluation by peak force and NMR spin-spin relaxation time. Postharvest Biol. Technol. 44, 157–164.

Valero, C., Crisosto, C.H., Slaughter, D.S., 2007. Relationship between nondestructive firmness measurements and commercially important ripening fruit stages for peaches, nectarines and plums. Postharvest Biol. Technol. 44, 248–253.